Gate controlled quantum interference: direct observation of anti-resonances in single molecule charge transport

Yueqi Li[1], Marius Buerkle[3], Guangfeng Li[4], Ali Rostamian[1], Hui Wang[2], Zixiao Wang[2], David R. Bowler[5,6], Tsuyoshi Miyazaki[7], Yoshihiro Asai*[3], Gang Zhou*[4] and Nongjian Tao*[1,2]

[1]Biodesign Center for Bioelectronics and Biosensors, Arizona State University, Tempe, Arizona 85287-5801, United States

[2]State Key Laboratory of Analytical Chemistry for Life Science, School of Chemistry and Chemical Engineering, Nanjing University, Nanjing 210023 (China).

[3]Research Center for Computational Design of Advanced Functional Materials (CD-FMat), National Institute of Advanced Industrial Science and Technology (AIST), Central 2, Umezono 1-1-1, Tsukuba, Ibaraki 305-8568, Japan

[4] Laboratory of Advanced Materials, State Key Laboratory of Molecular Engineering of Polymers, Fudan University, Shanghai 200438, P.R. China

[5] London Centre for Nanotechnology and Department of Physics and Astronomy, University College London, London WC1E 6BT, United Kingdom

[6] International Centre for Materials Nanoarchitectonics (MANA), National Institute for Materials Science (NIMS), 1-1 Namiki, Tsukuba, Ibaraki 305-0044, Japan

[7] International Centre for Materials Nanoarchitectonics (MANA), National Institute for Materials Science (NIMS), 1-1 Namiki, Tsukuba, Ibaraki 305-0044, Japan

*Corresponding authors

Abstract

Quantum interference can profoundly affect charge transport in single molecules, but experiments can usually measure only the conductance at the Fermi energy. Because in general the most pronounced features of the quantum interference are not located at the

Fermi energy, only the residual effects are observed to date. Here we not only measure the conductance but also map, using an electrochemical gate, the transmission functions at and around the Fermi energy and study signatures associated with constructive and destructive interference in single molecules directly. With the gate control, we tune the quantum interference between the highest occupied molecular orbital (HOMO) and lowest unoccupied molecular orbital (LUMO), reveal the anti-resonance, a distinct feature of destructive interference, and continuously control the conductance over 2 orders of magnitude by tuning the molecule in and out of the anti-resonance.

As devices decrease to the scale of the electronic phase coherence length, the wave nature of electrons becomes evident.[1-2] It is of both scientific and technological importance to study electron wave-interference and manipulate single molecule conductance at the level of the wave function. The interference between the highest occupied molecular orbital (HOMO) and lowest unoccupied molecular orbital (LUMO) is often the most dominant effect on the conductance of a single molecule.[3-4] Based on this, orbital rules have been proposed theoretically[5-7] and examined experimentally,[8-12] showing a constructive interference in linear conjugated (or para oriented) structures and a destructive interference in cross conjugated (or meta oriented) structures. However, these studies have focused on demonstrating quantum interference by designing molecules with different structures or modifying the structures via chemical reactions.[10, 13-16] Here we show that the charge transport controlled by the quantum interference in a single molecule can be tuned continuously with an external gate without changing the molecule structurally (Fig. 1a). This allows us to achieve gate control of single molecule conductance, to measure the transmission function of the molecule, and to study directly the most pronounced quantum interference features, including the destructive interference characteristic anti-resonance, in the transmission function.

We studied a meta-oriented diphenyl benzene structure (denoted as Meta), where substituents occupy positions 1 and 3, and a para-oriented diphenyl benzene structure (denoted as Para), where substituents occupy opposite sites (Fig. 1b). These molecules are connected to the two electrodes and studied using the scanning tunneling microscope (STM) break junction technique[17] (Fig. 1a). We tuned the quantum interference in the molecules with an electrochemical gate voltage, determined the conductance vs. gate voltage (transmission functions) and current-voltage characteristic

curves, performed theoretical calculations of the transmission functions, and compared the results with the experiments.

Results and Discussion

For a small bias voltage, the conductance (G) of a single molecule junction is given by the Landauer formula,

$$G(E_F) = \frac{2e^2}{h} T(E_F), \quad (1)$$

where e is the electron charge, h the Planck constant, and $T(E_F)$ the electron transmission function evaluated at the electrode Fermi energy, E_F. Quantum interference affects the transmission function, and thus the conductance of the molecule. For the Para and Meta molecules, the quantum effect can be understood intuitively by including only the frontier orbitals (HOMO and LUMO) in the zeroth order Green function,[4-5]

$$\frac{C_{H(\beta)}C_{H(\alpha)}^*}{E_F - \varepsilon_H} + \frac{C_{L(\beta)}C_{L(\alpha)}^*}{E_F - \varepsilon_L}, \quad (2)$$

where $C_{H,L(\alpha)}$ and $C_{H,L(\beta)}$ are the molecular orbital coefficients of HOMO (H) and LUMO (L) at the two anchoring atoms, α and β, connected to the two electrodes, and $\varepsilon_{H,L}$ is the molecular orbital energy of the HOMO (H) and LUMO (L). The square of the Green function is roughly proportional to transmission function (Eq. S2) and the interference is determined by the inter-orbit coupling induced by the electrodes.[9] By considering the phases of the frontier orbitals at the anchoring atoms shown in Fig. 1c, we conclude that the signs of the numerators in Eq. 2 to be the opposite for Para and same for Meta. The signs of the denominator on the other hand are always opposite

given that the Fermi energy lies within the HOMO-LUMO gap.[9] Hence the HOMO and LUMO contributions to the conductance add up for Para, resulting in constructive interference, and cancel out for Meta, leading to destructive interference.

When a gate voltage, V_g is applied to the molecule, the electrode Fermi level shifts relative to the molecule's HOMO and LUMO levels (Fig. 1d). This shift in the energy level alignment will influence the contribution from the inter-orbital coupling term between the HOMO and LUMO,[9] and thus the quantum interference in the molecules. In this way, the energy dependence of the transmission functions can be probed by continuously tuning the gate voltage.[18] For Meta, an anti-resonance in the transmission function located inside the HOMO-LUMO gap is predicted. As a result, the transmission function of Meta displays a strong energy dependence. In contrast, for para, the transmission function is in absence of an anti-resonance within the HOMO-LUMO gap and is expected to be less energy dependent. The intuitive model qualitatively agrees with more sophisticated theories,[9, 19-20] and also detailed first principle calculations presented later.

We note that electrochemical gating has been already previously applied to study charge transport in molecules previously.[10, 13, 16] In these works, however, chemical reactions took place, which changed not only the molecular structures, but also the HOMO and LUMO of the molecules. In contrast, the electrochemical gate in the present work changed merely the contribution from the HOMO and LUMO inter-orbital coupling term which determines the quantum interference[21-24], while the structures and the HOMO and LUMO of the molecules remained unchanged. This allowed us to continuously tune the quantum interference in the single molecules studied here.

Both isomers (Para and Meta) are terminated with two iodine atoms. Previous works[25-26] and our XPS study (Supplementary Fig. 1S) indicated that the iodine terminals could bind covalently with the gold electrodes and form molecular junctions (electrode-molecule-electrode). We performed STM break junction measurements[17, 27] [27]using a gold tip and substrate electrodes to investigate the conductance of single Para and Meta molecules (see details in Methods). The experiments generated thousands of conductance vs. distance traces, some showing plateaus associated with the formation of single molecule junctions, followed by abrupt drops corresponding to the breakdown of the junctions. As plotted in Figs. 2a and 2b, the plateaus measured for Para are located at higher conductance values than those for Meta. For statistical analysis of the conductance, we constructed conductance histograms from about ~700 of such individual traces for the two molecules (Figs. 2c and 2d). The conductance histograms exhibit broad peaks, where the peak positions represent the average conductance values of single molecules, which is $(2.8\pm0.2)\times10^{-4}$ G_0 for Para, and $(8.6\pm0.2)\times10^{-5}$ G_0 for Meta, where G_0 ($\frac{2e^2}{h}$=7.768$\times10^{-5}$ S) is the conductance quantum.

Because both Para and Meta consist of three phenyl rings connected by C-C bond, and terminated with iodine, the observed large conductance for Para and small conductance for Meta reflect constructive and destructive interference in the two molecules. As a control, we performed the same measurement in pure mesitylene in absence of Para or Meta. In the control experiment, the conductance traces did not show obvious plateaus, and the conductance histogram shows no obvious peaks (Supplementary Fig. 2), confirming that the conductance peaks in Figs. 2c and 2d are from Para and Meta.

To further investigate the quantum interference effect on the charge transport through the molecules, we determined I-V characteristics of the two molecules. This was achieved by first bridging a molecule between the STM tip and substrate electrodes, and then scanning the bias voltage between –2 V to 2 V while recording the current through the molecule (Methods).[28] By repeating the procedure, we recorded over a thousand of such I-V curves and constructed a 2D I-V histogram for each molecule. The I-V curves show that the current increases linearly with the bias within a small bias voltage range and increases rapidly at high bias voltages for both Para and Meta (Figs. 3a and 3b). An important observation is that the linear range for Para is larger than that for Meta. This difference is more clearly observed in the 2D histograms of conductance vs. bias voltage (Figs. 3c and 3d), which were obtained from the derivatives of the individual I-V curves. For Para, the 2D conductance histogram (Fig. 3c) shows a relatively shallow dependence of the conductance on the bias voltage. In contrast, the 2D conductance histogram of the Meta molecule exhibits a much steeper dependence (Fig. 3d). This observation reflects a key difference in the transmission functions of the Para and Meta molecules.[29]

To determine the transmission functions and examine quantum interference vs. energy, we shifted the energy alignment between the molecular orbital levels and the electrode Fermi level[30] with an electrochemical gate (Fig. 1d) (see experimental details in Methods). This changed the relative contributions of the HOMO and LUMO as described by the two terms in Eq. 2 and allowed us to obtain the transmission functions of the molecules (Fig. 1d bottom). To apply an electrochemical gate voltage (V_g) to the molecules with the STM break junction method, we performed the measurement in 0.1 M $KClO_4$ aqueous solution (instead of mesitylene). The first step was to identify the

formation of a single molecule junction from the conductance plateau, and then sweep the gate voltage from 0 to 0.3 V while recording the conductance of the molecule.

The Para conductance is around 3×10^{-4} G_0, which is consistent with that measured in mesitylene, and it shows little dependence on V_g (Fig. 4a). The lack of gate dependence indicates a relative flat transmission function for Para within the energy range changed by the gate. In contrast, Meta exhibits a much stronger gate effect with the conductance increased from $\sim 1 \times 10^{-4}$ G_0 at V_g=0 V to $\sim 5 \times 10^{-4}$ G_0 at V_g=0.3 V (Fig. 4b). The strong gate effect reflects a sharp feature in the transmission function of Meta. The observed difference between Meta and Para are consistent with the I-V characteristics of the two molecules. This experiment demonstrates that the quantum interference can be tuned by changing the relative coupling between the HOMO and LUMO with an external electrochemical gate. Applying an electrochemical gate voltage to a molecule is known to lead to oxidation or reduction of the molecules.[10, 13, 16, 30-31] To show that the electrochemical gate control of quantum interference in the present system did not involve the redox reactions, we measured cyclic voltammetry (CV) of both Para and Meta adsorbed on gold electrodes and did not observe the characteristic oxidation and reduction peaks associated with redox reactions (Supplementary Fig. 3).

Performing single molecule conductance vs. gate voltage measurements described above required a molecule bridged between the STM tip and substrate electrodes to be mechanically stable during the sweep of the gate voltage. We found that the molecule became increasingly unstable at large gate voltages (negative or positive), which limited the range of the applied gate voltage in the above single molecule measurement. To determine the conductance and transmission functions over

a broader energy range, we performed conductance measurement quickly and repeatedly to obtain a large number transient conductance curves at each fixed gate voltage and constructed conductance histograms at different gate voltages for both Para and Meta.[32] From the peaks in these conductance histograms, we obtained the average conductance values of single molecules vs. gate voltage. Because each measurement was transient, we were able to determine conductance at gate voltage from -0.55 V to 0.295 V using this approach. For Para, the conductance histogram peak increases from 1.4×10^{-4} G_0 to 3.9×10^{-4} G_0, a 2-3 folds conductance increase (Fig. 5a, and Supplementary Fig. 4). However, for Meta, the conductance increases from 2.5×10^{-6} G_0 to 4.7×10^{-4} G_0 (Fig. 5b and Supplementary Fig. 5), which is ~200 times increase, much greater than that for Para. The conductance of Meta became too small to be measured when V_g was more negative than -0.55 V. The lower detection limit of the conductance was determined by the ionic leakage current of the STM tip (Supplementary Fig. 6).

Figure 5c summarizes the measured conductance vs. gate voltage for Para (black circles) and Meta (red circles), from which we draw several important conclusions. First, the conductance increases with gate voltage for both Para and Meta, suggesting that the Fermi level is located closer to the HOMO level than to the LUMO level in the absence of gate voltage. This observation is supported by the theoretical prediction of energy alignment for phenyl substituted benzene compounds[9], and the energy alignment information allows us to compare the experimental data with the calculations. Note that a positive electrochemical gate potential shifts the molecular level up with respect to the Fermi level, which is opposite from the traditional solid-state gate. Second, Meta exhibits a much stronger gate effect than Para, revealing a pronounced difference in the transmission function between destructive and

9

constructive interference. Third, the sharp drop in the conductance of Meta as the gate voltage decreases to -0.6 V is the signature anti-resonance in the transmission function. Finally, the conductance vs. energy curves of Para and Meta can be fitted by the transmission functions determined with the simple model sketched by Eq. 2 (dashed curves in Fig. 5c).

To further validate the experimental data, we performed first-principle calculations of the Para and Meta molecules by combining the electronic structure derived from density functional theory (DFT) with nonequilibrium Green's functions (see Supplementary Methods and Supplementary Fig. 9) including an approximate self-energy correction to account for the over estimation of the electronic conductance.[33-34] We show two typical molecule-electrode contact geometries for Para and Meta in Fig. 6a, where OS represents the geometry with the dihedral angle between the two Au-I bonds at 0 degree, and SS represents the geometry with that dihedral angle at 180 degrees. The corresponding transmission functions of the two molecules with OS and SS geometries are given in Fig. 6b. At the Fermi energy, Para displays a more than one order of magnitude larger conductance ($G_{para}^{DFT+\Sigma} = 5.8 \times 10^{-4} G_0$) than Meta ($G_{meta}^{DFT+\Sigma} = 1.2 \times 10^{-5} G_0$), which agrees with the measured conductance for Para, but underestimates the one for Meta, though still within a reasonable range. The transmission functions of Para show relative small energy dependence within -1 and +1 V for both OS and SS contact geometries. In contrast, the transmission functions of Meta show much deeper energy dependence, and a signature of anti-resonance, which are in agreement with the experimental data. The transmission function of Meta is also more sensitive to the contact geometry. For OS, the transmission spectrum is approximately symmetric with respect to the HOMO and LUMO resonance, and the anti-resonance locates in the center of the HOMO-LUMO gap. However, the

transmission spectrum for SS is asymmetric with the anti-resonance shifted towards the HOMO. The exact contact geometries of the molecules remain unknown, but the first principle calculations provide a good prediction of the basic anti-resonance feature regardless of the detailed geometry.

Conclusions

We have archived continuous control of quantum interference in single molecules by electrochemical gating and studied its effect on the charge transport behaviors. The gate voltage tunes the relative coupling strength between the HOMO and LUMO, and leads to different conductance dependence on gate for molecules with constructive interference and destructive interference. By measuring the conductance vs. gate voltage, we have determined the transmission functions of the molecules, and observed the anti-resonance, which is a distinct signature of destructive interference, and its presence allows gate control of conductance over 2 orders of magnitude. We have further performed calculations to confirm and rationalize the experimental findings. This work provides a direct observation of quantum interference in charge transport and demonstrates continuous tuning of single molecule conductance with an external gate, a unique device function based on quantum effect.

Materials and methods

<u>Synthesis of Para and Meta</u>

All reactions and manipulations were carried out under the standard inert atmosphere and using the Schlenk techniques. Anhydrous toluene was distilled from sodium

benzophenone ketyl and anhydrous dichloromethane (DCM) was distilled from CaH_2. Stainless steel syringes were used to transfer these moisture-sensitive solvents. 1,3-Dibromobenzene, 1,4-dibromobenzene, trimethylsilylphenylboronic acid, and iodine monochloride were purchased from J&K Chemical, Ltd. Proton nuclear magnetic resonance (^{1}H NMR, 400 MHz) spectra and carbon nuclear magnetic resonance (^{13}C NMR, 100 MHz) spectra were measured on a Varian Mercury Plus-400 spectrometer. The chemical shifts were in parts per million downfield from tetramethylsilane (TMS) and $CDCl_3$. The splitting patterns are designated as follows: s (singlet); d (doublet); and m (multiplet).

Synthesis of 4,4''-bis(trimethylsilyl)-1,1':3',1''-terphenyl.

Under an argon atmosphere, a mixture of 1,3-dibromobenzene (1.00 g, 4.27 mmol), trimethylsilylphenylboronic acid (1.82 g, 9.40 mmol), K_2CO_3 (2.77 g, 20.44 mmol), and $Pd(PPh_3)_4$ (0.25 g, 0.22 mmol) in a mixed solvent of toluene (20 mL) and water (10 mL) was stirred and heated at 85 °C for 8 h. Then the mixture was cooled to room temperature, extracted with diethyl ether, and washed with water. The separated organic layer was dried over anhydrous $MgSO_4$. After removal of the solvent by evaporation, the residue was purified by column chromatography on silica gel to afford the desired white product (0.76 g, yield: 48%). ^{1}H NMR (400 MHz, $CDCl_3$, δ ppm): 7.84 (s, 1H), 7.63 (s, 8H), 7.59 (d, $J = 7.2$ Hz, 2H), 7.51 (m, 1H), 0.32 (s, 18H). ^{13}C NMR (100 MHz, $CDCl_3$, δ ppm): 141.96, 141.78, 139.65, 134.08, 129.40, 126.81, 126.42, 126.37, -0.85.

Synthesis of 4,4''-diiodo-1,1':3',1''-terphenyl (Meta).

Iodine monochloride (2.5 mL of 1.0 M solution in CH_2Cl_2) was added to a solution of 4,4''-bis(trimethylsilyl)-1,1':3',1''-terphenyl (300 mg, 0.8 mmol) in CH_2Cl_2 (10 mL) at 0 °C under an argon atmosphere. The reaction mixture was stirred at room temperature for 12 h. $NaHSO_3$ aqueous solution was then added to remove unreacted iodine monochloride. The organic layer was separated and dried over anhydrous $MgSO_4$. The solvent was removed in a rotary vacuum evaporator, and the residue was chromatographed on a silica gel column to give white solid (220 mg, 58%). ^{1}H NMR (400 MHz, $CDCl_3$, δ ppm): 7.78 (d, $J = 8.4$ Hz, 4H), 7.70 (s, 1H), 7.55 – 7.51 (m, 3H), 7.38 (d, $J = 8.4$ Hz, 4H). ^{13}C NMR (100 MHz, $CDCl_3$, δ ppm): 141.05, 140.67, 138.15, 129.72, 129.28, 126.47, 125.77, 93.55.

Synthesis of 4,4''-bis(trimethylsilyl)-1,1':4',1''-terphenyl.

Under an argon atmosphere, a mixture of 1,4-dibromobenzene (1.00 g, 4.27 mmol), trimethylsilylphenylboronic acid (1.82 g, 9.40 mmol), K_2CO_3 (2.77 g, 20.44 mmol), and $Pd(PPh_3)_4$ (0.25 g, 0.22 mmol) in a mixed solvent of toluene (20 mL) and water (10 mL) was stirred and heated at 85 °C for 8 h. Then the mixture was cooled to room temperature, extracted with diethyl ether, and washed with water. The separated organic layer was dried over anhydrous $MgSO_4$. After evaporation of the solvent, the residue was purified by column chromatography on silica gel to afford the desired product (0.93 g, yield: 58%). ^{1}H NMR (400 MHz, $CDCl_3$, δ ppm): 7.70 (s, 4H), 7.65 (s, 8H), 0.33 (s, 18H). ^{13}C NMR (100 MHz, $CDCl_3$, δ ppm): 141.30, 140.36, 139.59, 134.12, 127.75, 126.61, -0.82.

Synthesis of 4,4''-diiodo-1,1':4',1''-terphenyl (Para).

Iodine monochloride (2.5 mL of 1.0 M solution in CH_2Cl_2) was added to a solution of 4,4''-bis(trimethylsilyl)-1,1':3',1''-terphenyl (300 mg, 0.8 mmol) in CH_2Cl_2 (10 mL) at 0 °C under an argon atmosphere. The reaction mixture was stirred at room temperature for 12 h. $NaHSO_3$ aqueous solution was then added to remove unreacted iodine monochloride. The organic layer was separated and dried over anhydrous $MgSO_4$. The solvent was removed in a rotary vacuum evaporator, and the residue was chromatographed on a silica gel column to give white solid (264 mg, 68%). ^{1}H NMR (400 MHz, $CDCl_3$, δ ppm): 7.77 (d, J = 8.4 Hz, 4H), 7.63 (s, 4H), 7.38 (d, J = 8.4 Hz, 4H). The solubility of the target compound was too low to perform ^{13}C NMR measurement. (^{1}H NMR spectra of Meta and Para in $CDCl_3$ are presented in Supplementary Figs. 7 and 8.)

Immobilization of Para and Meta on gold electrodes

Para and Meta were immobilized on a gold thin film electrode (with ~160 nm gold on mica) prepared with a vapor deposition system under ultrahigh vacuum. Before each experiment, the gold substrate was annealed with hydrogen flame briefly, immersed in mesitylene (Sigma-Aldrich, 98%) containing 30 μM Para or Meta, incubated overnight, then rinsed with mesitylene and dried with nitrogen gas. We bubbled the aqueous solution of 50 mM $KClO_4$ (Sigma-Aldrich, 99%) for 3 hours to purge oxygen, then added the solution on top of the Para or Meta-covered gold film in a glove box under nitrogen atmosphere.

Measurement of single molecule conductance

The electrochemical gate-controlled break junction measurements were carried out by an electrochemical scanning tunneling microscope (EC-STM) consisting of a controller (Nanoscope E, digital Instruments), a STM scanner (Molecular Imaging) and a bipotentiostat (Agilent). For each experiment, the STM tip was freshly prepared by cutting a gold wire (0.25 mm diameter, 99.5%). For electrochemical gate control, the tip was coated with Apiezon wax to reduce ionic leakage current. A silver wire and platinum coil were used as quasi-reference electrode and counter electrode, respectively.

We performed the STM break junction measurements with the following three approaches. In the first approach, the sample was measured in mesitylene solution of 30 μM Para/Meta without applying gate potential[17]. A small bias (100 mV) was applied between the STM tip and substrate electrodes. The STM tip was repeatedly brought into contact and retracted from the substrate, during which thousands of conductance distance traces (Figs. 2a and 2b) were collected to construct conductance histograms (Figs. 2c and 2d). In the second approach, a quasi-reference electrode (silver wire) and a counter electrode (platinum coil) were inserted in 50 mM $KClO_4$ aqueous solution to allow gate-controlled conductance measurement. The break junction measurement was carried out in the same way as the first approach with the gate voltage held at a fixed value ranging from -0.5 V to 0.3 V[32]. The experiments were conducted in a glovebox under nitrogen atmosphere. In the third approach, instead of applying a fixed gate voltage, we studied the conductance of a molecule while sweeping the gate voltage[30]. We fixed the tip-substrate bias at 0. 1 V and the initial gate voltage at 0 V and perform break junction measurement. Once a plateau at single molecule conductance level was detected automatically with a LabView program, signaling the formation of a single

molecule junction, the tip was held in position and the potential was scanned at 1 V/s to record the conductance vs. potential (Fig. 4).

Measurement of single molecule current-voltage characteristics

First, we carried out the break junction measurement in mesitylene solution containing either Para or Meta. When a molecule was bridge between the STM tip and the gold film, a plateau appeared in the conductance vs. distance trace, the tip was held in position and the bias was swept between -2 V to 2 V in 0.1 s to record an current-voltage characteristic curve.[28] We repeated the procedure to obtain thousands of individual current-voltage characteristic curves. From each current-voltage characteristic curve, we extract a conductance-voltage curve. We constructed 2D histograms of current-voltage characteristics (Figs.3a and 3b) and conductance-voltage curves (Figs.3c and 3d) from more than one thousand individual curves.

Supplementary Information:

Supplementary Figures 1-9

Supplementary Computational Methods

References

1.   Solomon, G. C.; Andrews, D. Q.; Hansen, T.; Goldsmith, R. H.; Wasielewski, M. R.; Van Duyne, R. P.; Ratner, M. A., Understanding quantum interference in coherent molecular conduction. *The Journal of Chemical Physics* **2008,** *129* (5), 054701.
2.   Aradhya, S. V.; Venkataraman, L., Single-molecule junctions beyond electronic transport. *Nat Nano* **2013,** *8* (6), 399-410.
3.   Yoshizawa, K.; Tada, T.; Staykov, A., Orbital Views of the Electron Transport in Molecular Devices. *Journal of the American Chemical Society* **2008,** *130* (29), 9406-9413.
4.   Tada, T.; Yoshizawa, K., Molecular design of electron transport with orbital rule: toward conductance-decay free molecular junctions. *Physical Chemistry Chemical Physics* **2015,** *17* (48), 32099-32110.
5.   Yoshizawa, K., An Orbital Rule for Electron Transport in Molecules. *Accounts of Chemical Research* **2012,** *45* (9), 1612-1621.
6.   Markussen, T.; Stadler, R.; Thygesen, K. S., The Relation between Structure and Quantum Interference in Single Molecule Junctions. *Nano Letters* **2010,** *10* (10), 4260-4265.
7.   Cardamone, D. M.; Stafford, C. A.; Mazumdar, S., Controlling Quantum Transport through a Single Molecule. *Nano Letters* **2006,** *6* (11), 2422-2426.
8.   Manrique, D. Z.; Huang, C.; Baghernejad, M.; Zhao, X.; Al-Owaedi, O. A.; Sadeghi, H.; Kaliginedi, V.; Hong, W.; Gulcur, M.; Wandlowski, T.; Bryce, M. R.; Lambert, C. J., A quantum circuit rule for interference effects in single-molecule electrical junctions. **2015,** *6,* 6389.
9.   Bürkle, M.; Xiang, L.; Li, G.; Rostamian, A.; Hines, T.; Guo, S.; Zhou, G.; Tao, N.; Asai, Y., The Orbital Selection Rule for Molecular Conductance as Manifested in Tetraphenyl-Based Molecular Junctions. *Journal of the American Chemical Society* **2017,** *139* (8), 2989-2993.
10.   Koole, M.; Thijssen, J. M.; Valkenier, H.; Hummelen, J. C.; Zant, H. S. J. v. d., Electric-Field Control of Interfering Transport Pathways in a Single-Molecule Anthraquinone Transistor. *Nano Letters* **2015,** *15* (8), 5569-5573.
11.   Aradhya, S. V.; Meisner, J. S.; Krikorian, M.; Ahn, S.; Parameswaran, R.; Steigerwald, M. L.; Nuckolls, C.; Venkataraman, L., Dissecting Contact Mechanics from Quantum Interference in Single-Molecule Junctions of Stilbene Derivatives. *Nano Letters* **2012,** *12* (3), 1643-1647.
12.   Guedon, C. M.; Valkenier, H.; Markussen, T.; Thygesen, K. S.; Hummelen, J. C.; van der Molen, S. J., Observation of quantum interference in molecular charge transport. *Nat Nano* **2012,** *7* (5), 305-309.
13.   Baghernejad, M.; Zhao, X.; Baruël Ørnsø, K.; Füeg, M.; Moreno-García, P.; Rudnev, A. V.; Kaliginedi, V.; Vesztergom, S.; Huang, C.; Hong, W.; Broekmann, P.; Wandlowski, T.; Thygesen, K. S.; Bryce, M. R., Electrochemical Control of Single-Molecule Conductance by Fermi-Level Tuning and Conjugation Switching. *Journal of the American Chemical Society* **2014,** *136* (52), 17922-17925.
14.   Baer, R.; Neuhauser, D., Phase Coherent Electronics: A Molecular Switch Based on Quantum Interference. *Journal of the American Chemical Society* **2002,** *124* (16), 4200-4201.
15.   Liu, X.; Sangtarash, S.; Reber, D.; Zhang, D.; Sadeghi, H.; Shi, J.; Xiao, Z.-Y.; Hong, W.; Lambert, C. J.; Liu, S.-X., Gating of Quantum Interference in Molecular Junctions by Heteroatom Substitution. *Angewandte Chemie International Edition* **2017,** *56* (1), 173-176.

16.   Darwish, N.; Díez-Pérez, I.; Da Silva, P.; Tao, N.; Gooding, J. J.; Paddon-Row, M. N., Observation of Electrochemically Controlled Quantum Interference in a Single Anthraquinone-Based Norbornylogous Bridge Molecule. *Angewandte Chemie International Edition* **2012,** *51* (13), 3203-3206.

17.   Xu, B.; Tao, N. J., Measurement of Single-Molecule Resistance by Repeated Formation of Molecular Junctions. *Science* **2003,** *301* (5637), 1221.

18.   Capozzi, B.; Low, J. Z.; Xia, J.; Liu, Z.-F.; Neaton, J. B.; Campos, L. M.; Venkataraman, L., Mapping the Transmission Functions of Single-Molecule Junctions. *Nano Letters* **2016,** *16* (6), 3949-3954.

19.   Mayor, M.; Weber, H. B.; Reichert, J.; Elbing, M.; von Hänisch, C.; Beckmann, D.; Fischer, M., Electric Current through a Molecular Rod—Relevance of the Position of the Anchor Groups. *Angewandte Chemie International Edition* **2003,** *42* (47), 5834-5838.

20.   Taniguchi, M.; Tsutsui, M.; Mogi, R.; Sugawara, T.; Tsuji, Y.; Yoshizawa, K.; Kawai, T., Dependence of Single-Molecule Conductance on Molecule Junction Symmetry. *Journal of the American Chemical Society* **2011,** *133* (30), 11426-11429.

21.   Ke, S.-H.; Yang, W.; Baranger, H. U., Quantum-Interference-Controlled Molecular Electronics. *Nano Letters* **2008,** *8* (10), 3257-3261.

22.   Hsu, L.-Y.; Chen, C.-Y.; Li, E. Y.; Rabitz, H., Gate Control of Artificial Single-Molecule Electric Machines. *The Journal of Physical Chemistry C* **2015,** *119* (9), 4573-4579.

23.   Lovey, D. A.; Romero, R. H., Quantum interference through gated single-molecule junctions. *Chemical Physics Letters* **2012,** *530*, 86-92.

24.   Li, Y.; Mol, J. A.; Benjamin, S. C.; Briggs, G. A. D., Interference-based molecular transistors. **2016,** *6*, 33686.

25.   Xiang, L.; Hines, T.; Palma, J. L.; Lu, X.; Mujica, V.; Ratner, M. A.; Zhou, G.; Tao, N., Non-exponential Length Dependence of Conductance in Iodide-Terminated Oligothiophene Single-Molecule Tunneling Junctions. *Journal of the American Chemical Society* **2016,** *138* (2), 679-687.

26.   Eder, G.; Smith, E. F.; Cebula, I.; Heckl, W. M.; Beton, P. H.; Lackinger, M., Solution Preparation of Two-Dimensional Covalently Linked Networks by Polymerization of 1,3,5-Tri(4-iodophenyl)benzene on Au(111). *ACS Nano* **2013,** *7* (4), 3014-3021.

27.   Li, Y.; Xiang, L.; Palma, J. L.; Asai, Y.; Tao, N., Thermoelectric effect and its dependence on molecular length and sequence in single DNA molecules. *Nature Communications* **2016,** *7*, 11294.

28.   Guo, S.; Hihath, J.; Díez-Pérez, I.; Tao, N., Measurement and Statistical Analysis of Single-Molecule Current–Voltage Characteristics, Transition Voltage Spectroscopy, and Tunneling Barrier Height. *Journal of the American Chemical Society* **2011,** *133* (47), 19189-19197.

29.   Cai, Z.; Lo, W.-Y.; Zheng, T.; Li, L.; Zhang, N.; Hu, Y.; Yu, L., Exceptional Single-Molecule Transport Properties of Ladder-Type Heteroacene Molecular Wires. *Journal of the American Chemical Society* **2016,** *138* (33), 10630-10635.

30.   Xiao, X.; Nagahara, L. A.; Rawlett, A. M.; Tao, N., Electrochemical Gate-Controlled Conductance of Single Oligo(phenylene ethynylene)s. *Journal of the American Chemical Society* **2005,** *127* (25), 9235-9240.

31.   Li, Y.; Haworth, N. L.; Xiang, L.; Ciampi, S.; Coote, M. L.; Tao, N., Mechanical Stretching-Induced Electron-Transfer Reactions and Conductance Switching in Single Molecules. *Journal of the American Chemical Society* **2017,** *139* (41), 14699-14706.

32.   Xiang, L.; Palma, J. L.; Li, Y.; Mujica, V.; Ratner, M. A.; Tao, N., Gate-controlled conductance switching in DNA. *Nature Communications* **2017,** *8*, 14471.

33.   Zotti, L. A.; Bürkle, M.; Pauly, F.; Lee, W.; Kim, K.; Jeong, W.; Asai, Y.; Reddy, P.; Cuevas, J. C., Heat dissipation and its relation to thermopower in single-molecule junctions. *New Journal of Physics* **2014,** *16* (1), 015004.

34.   Quek, S. Y.; Khoo, K. H., Predictive DFT-Based Approaches to Charge and Spin Transport in Single-Molecule Junctions and Two-Dimensional Materials: Successes and Challenges. *Accounts of Chemical Research* **2014,** *47* (11), 3250-3257.
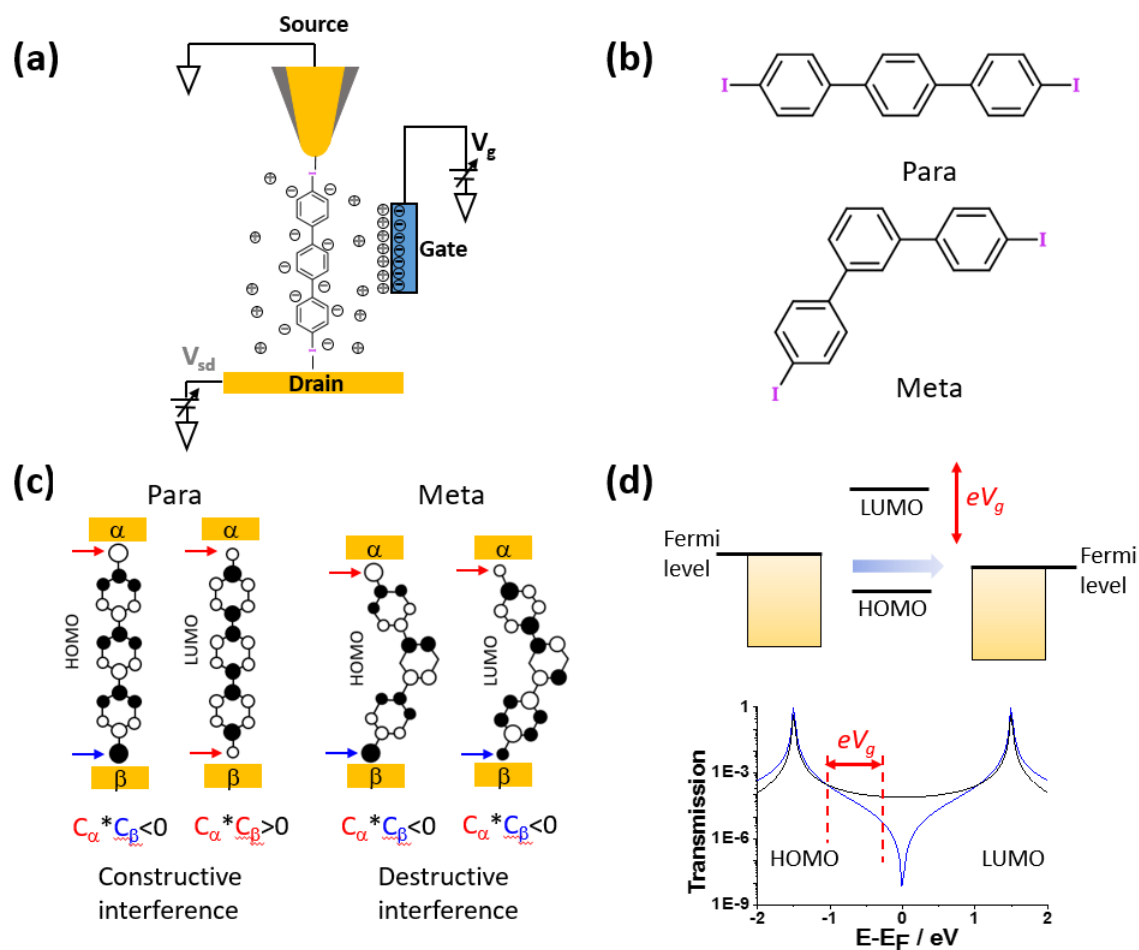
Figure 1. Para and Meta molecules measured by gate controlled STM break junction. (a) Schematic view of the gate-controlled measurement of single molecule charge transport. **(b)** Chemical structure of the molecules with constructive quantum interference (Para) and destructive quantum interference (Meta). **(c)** Schematic view of the frontier orbitals of Para and Meta. **(d)** Upper panel: adjusting the gate voltage shifts the molecular energy levels relative to the electrode' Fermi energy level, which varies the occupancy of the two interfering charge transport channels. Lower panel: adjusting the gate voltage changes the relative alignment between molecular energy levels and Fermi level, allowing probing of the energy dependence of transmission. The black and blue curves are representative transmission functions of constructive and destructive interference situations, respectively.
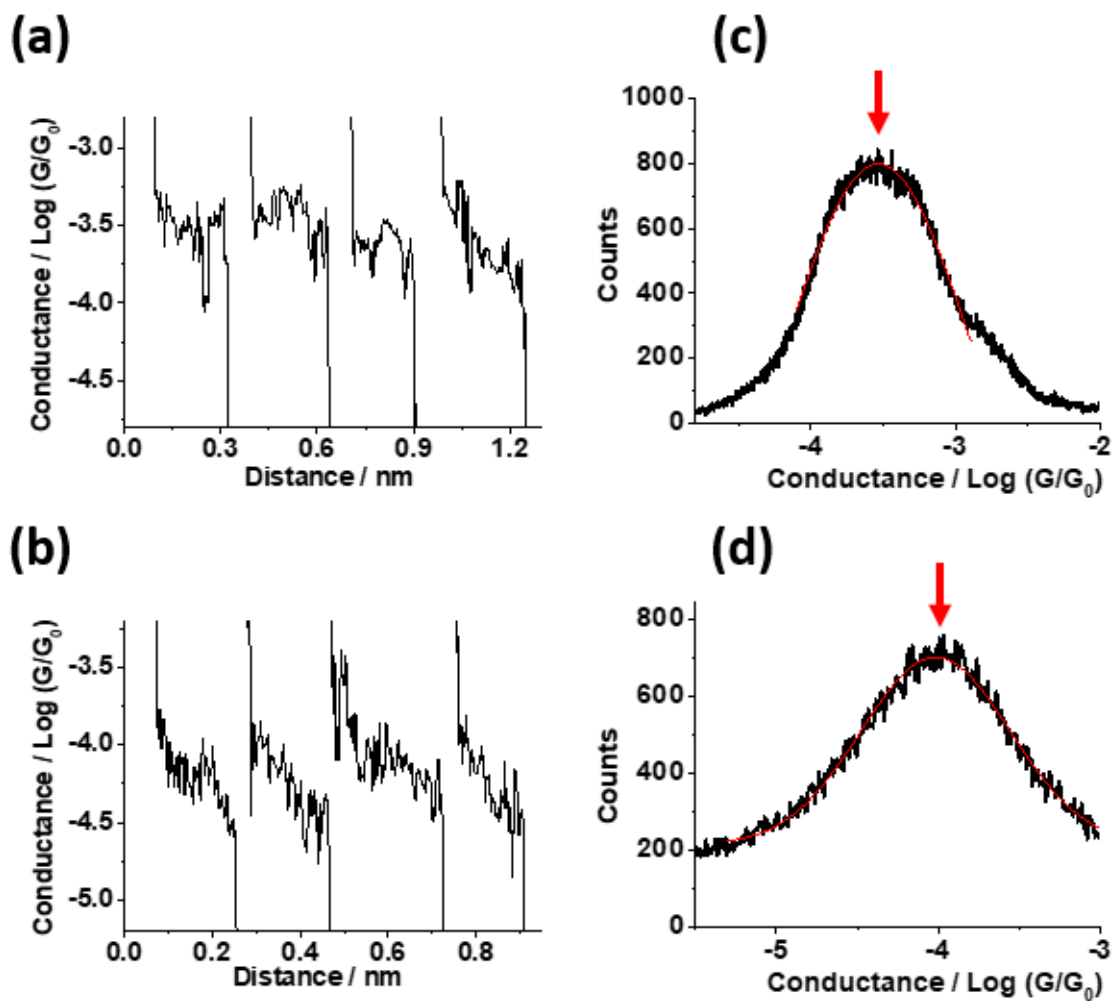
Figure 2. Conductance measurement of Para and Meta in mesitylene without gate applied. Individual conductance versus distance traces recorded from the break junction measurement of **(a)** Para and **(b)** Meta. Conductance histograms of **(c)** Para and **(d)** Meta constructed from individual curves. The red curves are Gaussian fitting of the conductance peaks. The peak positions are marked by red arrows.
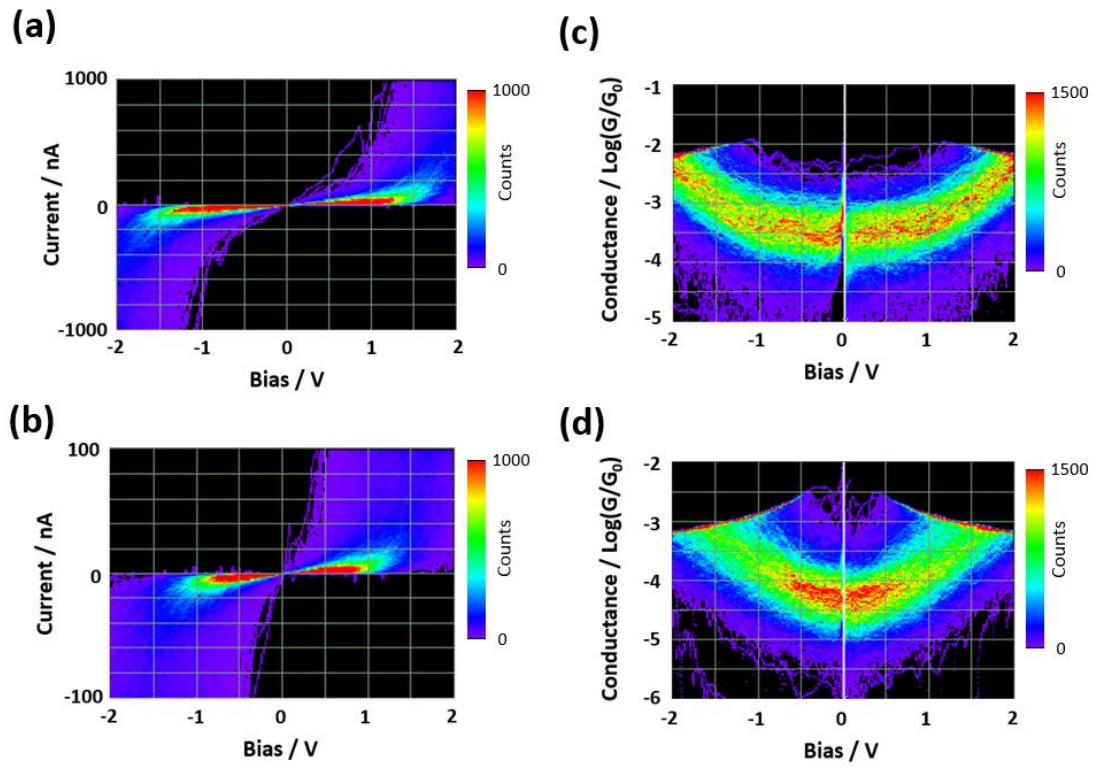
Figure 3. Current-voltage (I-V) characteristics of Para and Meta. 2D I-V histograms of **(a)** Para and **(b)** Meta. 2D conductance-voltage (G-V) histograms of **(c)** Para and **(d)** Meta. Each histogram consists of more than 1000 curves.
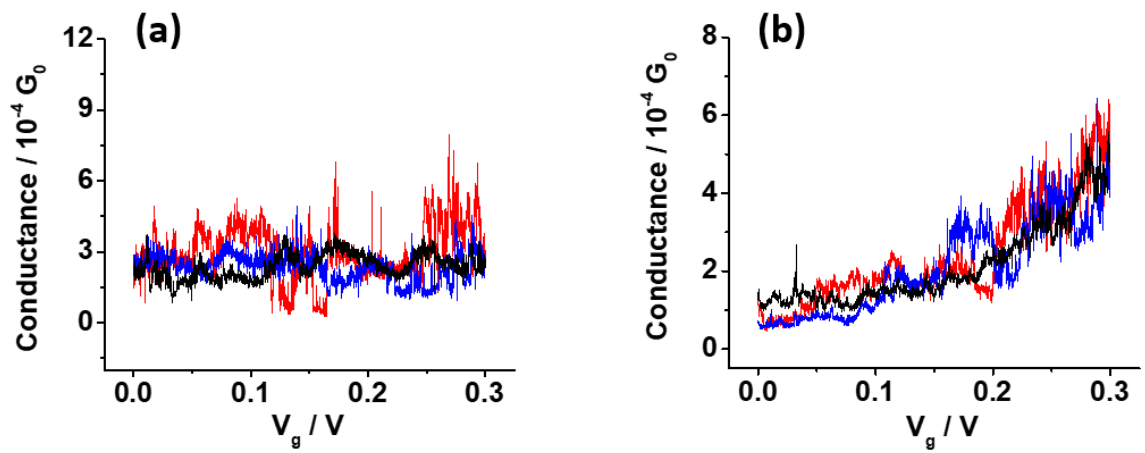
Figure 4. Conductance of (a) Para and (b) Meta versus gate potential (V_g) swept at 1 V/s, revealing a much larger gate dependency for the conductance of Meta than Para. Different colors represent different sweeps.
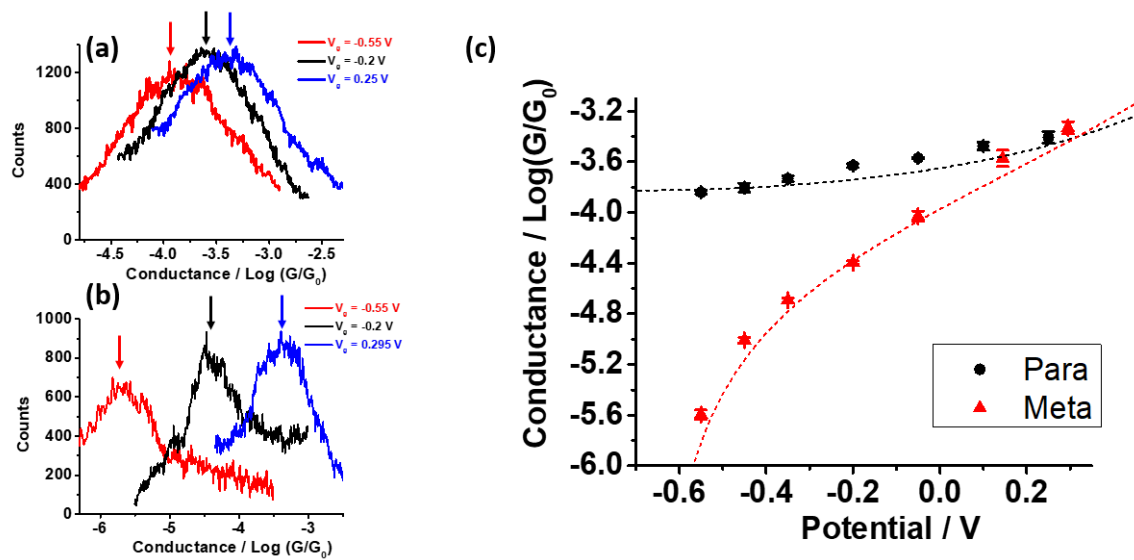
Figure 5. **Conductance of Para and Meta single molecules measured at different gate potentials. (a)** Conductance histograms of Para measured at gate potential of +0.25 V (blue), -0.2 V (black), and -0.55 V (red). **(b)** Conductance histograms of Meta measured at gate potential of +0.295 V (blue), -0.2 V (black), and -0.55 V (red). **(c)** Conductance of Para and Meta versus gate potential. The round black dots are for Para, and the red triangle dots are for Meta. The error bars are standard deviations of three independent measurements. The black/red dashed lines are fittings of the data by the simple constructive and destructive interference transmission functions (details given in the text).
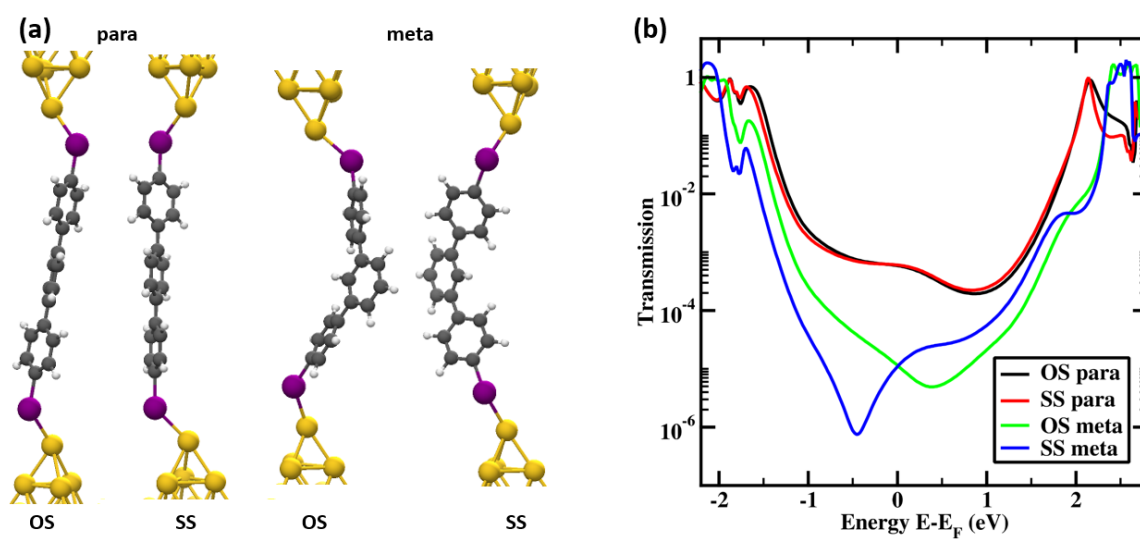
Figure 6. **Contact geometries and transmission functions.** (a) Typical contact geometries considered for the transport calculations. OS represents the geometry with the dihedral angle between the two Au-I bonds at 0 degree, and SS represents the geometry with that dihedral angle at 180 degrees. **(b)** Transmission function calculated for the different geometries of Para and Meta based on the DFT $+ \Sigma$ model.

Gate controlled quantum interference: direct observation of anti-resonances in single molecule charge transport

Yueqi Li[1], Marius Buerkle[3], Guangfeng Li[4], Ali Rostamian[1], Hui Wang[2], Zixiao Wang[2], David R. Bowler[5,6], Tsuyoshi Miyazaki[7], Yoshihiro Asai*[3], Gang Zhou*[4] and Nongjian Tao*[1,2]

[1]Biodesign Center for Bioelectronics and Biosensors, Arizona State University, Tempe, Arizona 85287-5801, United States

[2]State Key Laboratory of Analytical Chemistry for Life Science, School of Chemistry and Chemical Engineering, Nanjing University, Nanjing 210023 (China).

[3]Research Center for Computational Design of Advanced Functional Materials (CD-FMat), National Institute of Advanced Industrial Science and Technology (AIST), Central 2, Umezono 1-1-1, Tsukuba, Ibaraki 305-8568, Japan

[4] Laboratory of Advanced Materials, State Key Laboratory of Molecular Engineering of Polymers, Fudan University, Shanghai 200438, P.R. China

[5] London Centre for Nanotechnology and Department of Physics and Astronomy, University College London, London WC1E 6BT, United Kingdom

[6] International Centre for Materials Nanoarchitectonics (MANA), National Institute for Materials Science (NIMS), 1-1 Namiki, Tsukuba, Ibaraki 305-0044, Japan

[7] International Centre for Materials Nanoarchitectonics (MANA), National Institute for Materials Science (NIMS), 1-1 Namiki, Tsukuba, Ibaraki 305-0044, Japan

*Corresponding authors

Supplementary Figure 1. XPS analysis Para and Meta adsorbed on Au surfaces.
(a) I 3d analysis: Para shows a single peak at 619.5 eV with no feature at 621.3 eV, where the peak for an isolated I-C[1] is located, indicating that only Au-I-C bond[2] presents on the surface, and the iodine atoms at the ends of Para are bound to Au surface. **(b)** C 1s analysis: Para shows two peaks in this region, one at 296.0 eV for C-C/C-H bond[3], the other one at 286.8 eV is much lower in peak height and likely due to C-I bond[4]. No feature is shown for C-Au bond at 283 eV. The XPS spectrum indicates that carbon only binds with carbon or iodine, but not to Au. **(c)** Similar conclusion as in (a) can be drawn from the I 3d analysis of Meta. **(d)** Similar conclusion as in (b) can be drawn from the C 1s regime analysis of Meta. The bottom brown lines are nonlinear Shirley baselines.
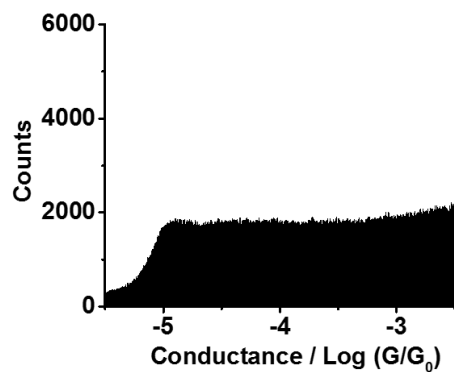
Supplementary Figure 2. Control experiment. Conductance histogram of conductance traces obtained in pure mesitylene, which shows no obvious peaks.
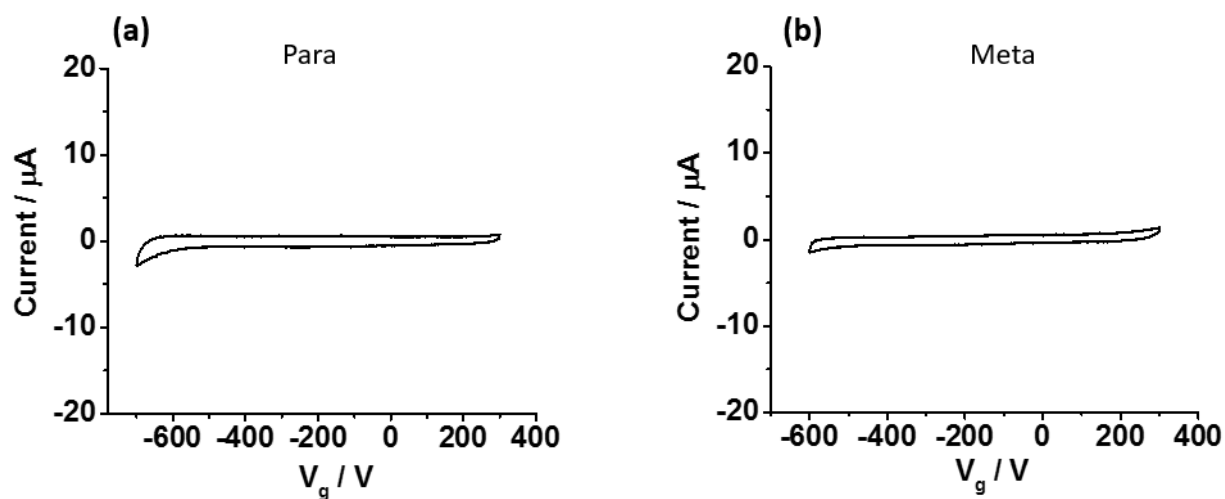
Supplementary Figure 3. **Absence of chemical reactions induced by the gate voltage.** Cyclic voltammograms (CV) of **(a)** Para and **(b)** Meta adsorbed on Au surface performed in 50 mM KClO$_4$ with potential sweep rate of 100 mV/s and using Ag wire as quasi reference electrode and Pt as counter electrode.
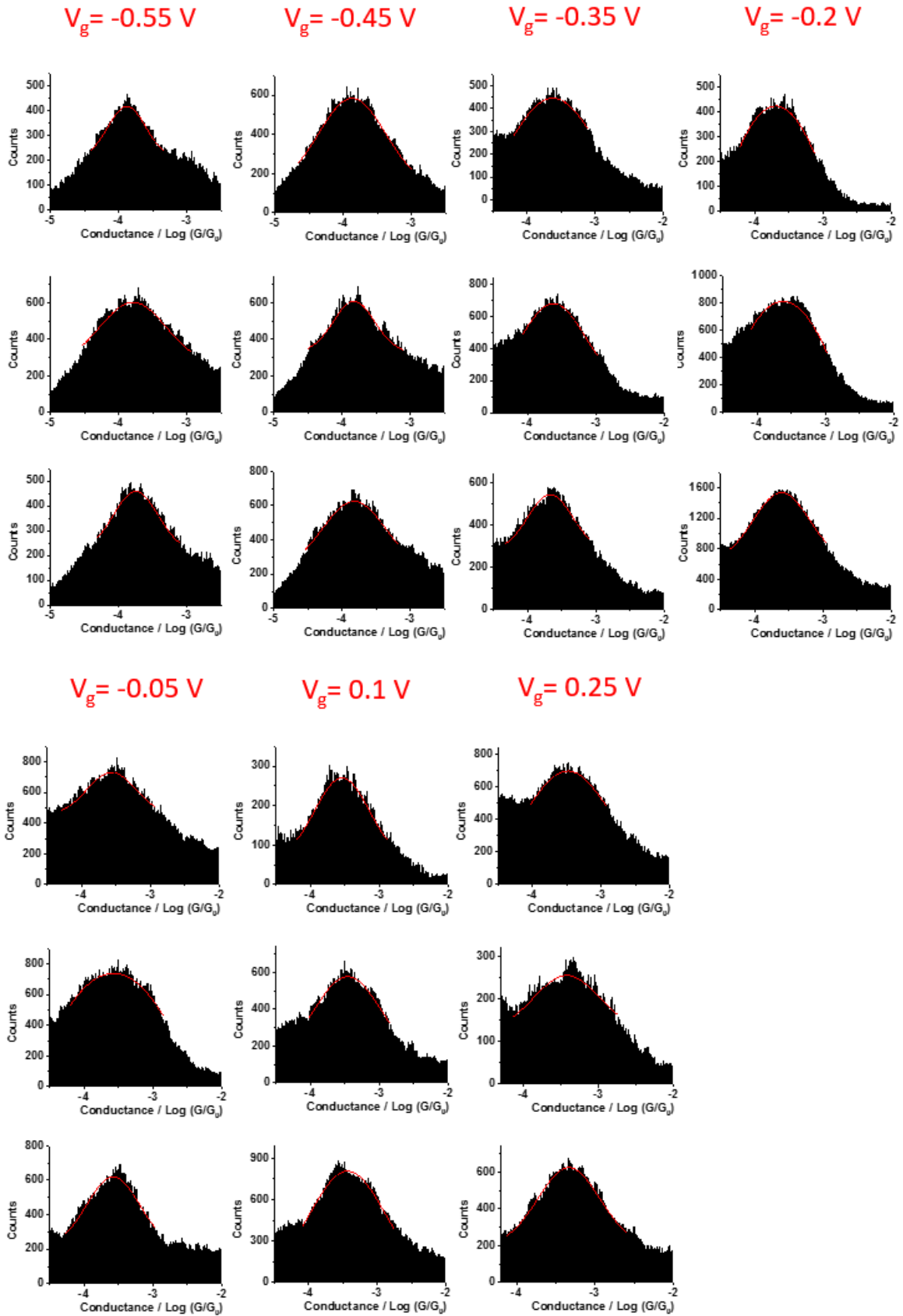
Supplementary Figure 4. **Conductance histograms of Para at different gate voltages** (V_g), where the red lines are Gaussian fittings of the peaks.

V_g= -0.55 V V_g= -0.45 V V_g= -0.35 V V_g= -0.2 V
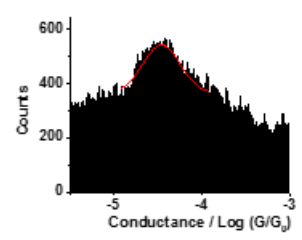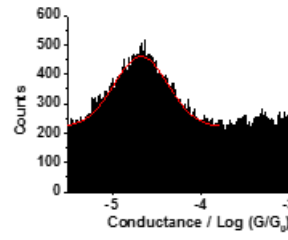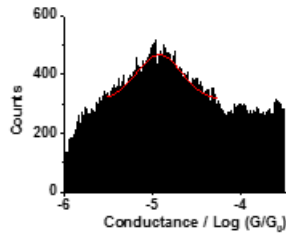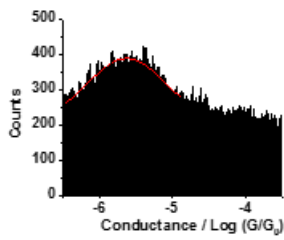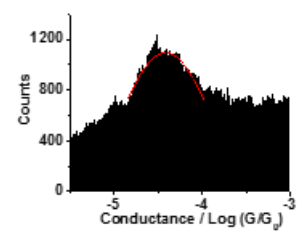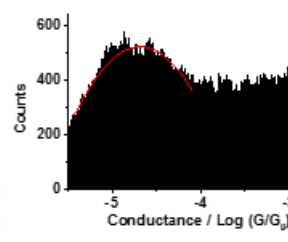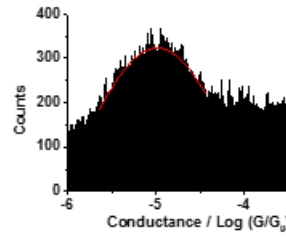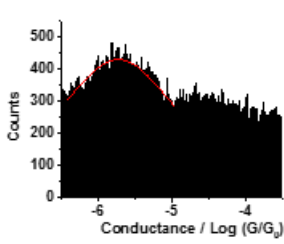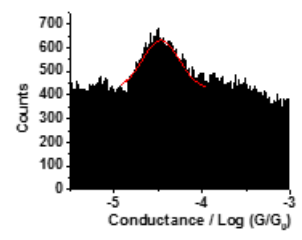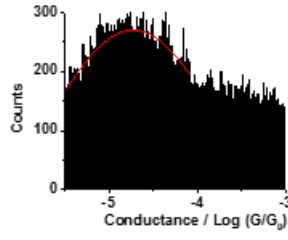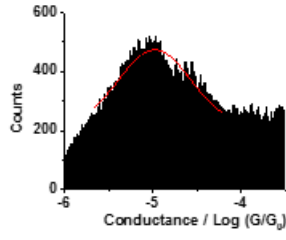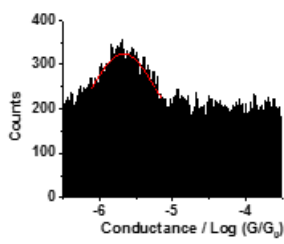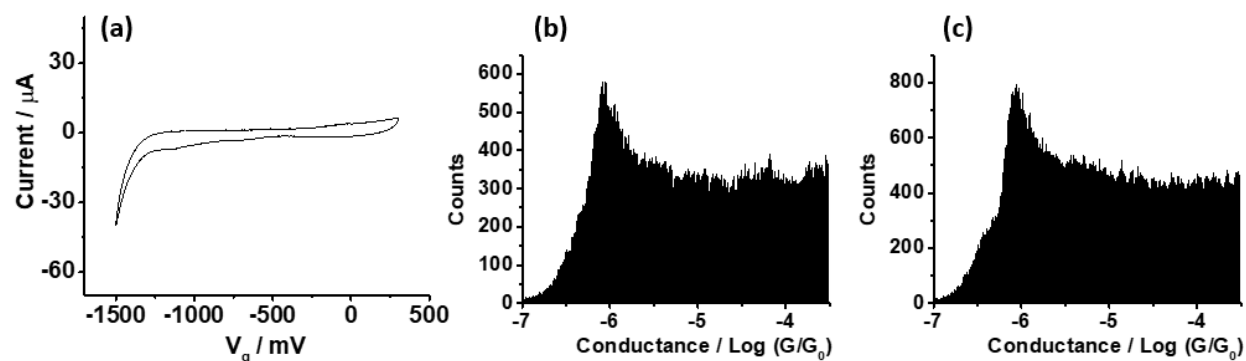
V_g= -0.05 V V_g= 0.145 V V_g= 0.295 V
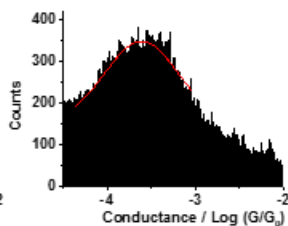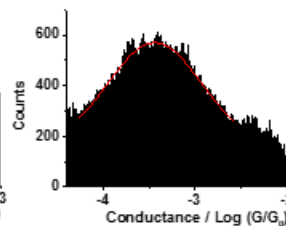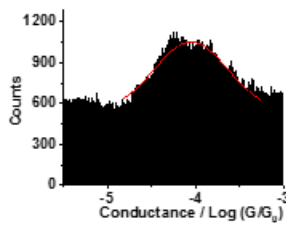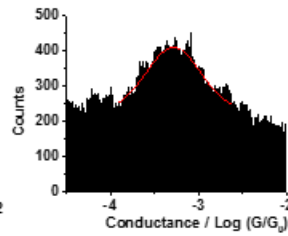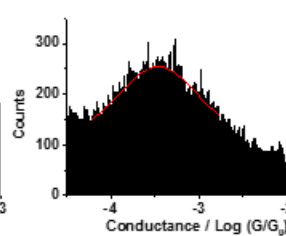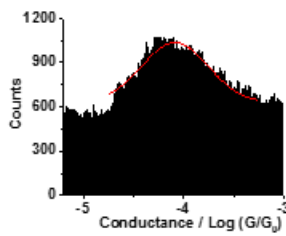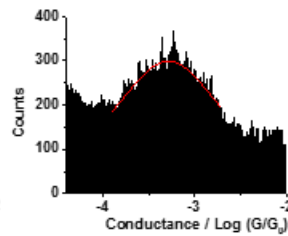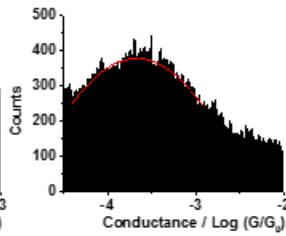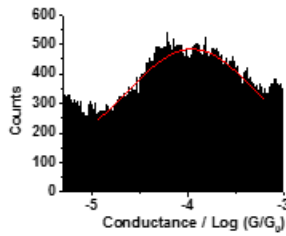
Supplementary Figure 5. Conductance histograms of Meta at different gate voltages (V_g), where the red lines are Gaussian fittings of the peaks. (The histograms at -0.55V were corrected with the leakage current)

Supplementary Figure 6. Conductance measurements at extremely positive and negative gate voltages. **(a)** Cyclic voltammogram performed with potential sweep rate of 100 mV/s in 50 mM $KClO_4$ with Ag quasi reference electrode and Pt counter electrode. Large faradaic current corresponding to redox reaction appears when the gate potential (V_g) is more negative than -1 V. **(b)** Conductance histogram of Meta at V_g= -0.65 V. The peak at -6 is due to leakage current. **(c)** Conductance histogram of Meta d at V_g= -1 V. The peak at -6 is due to leakage current.
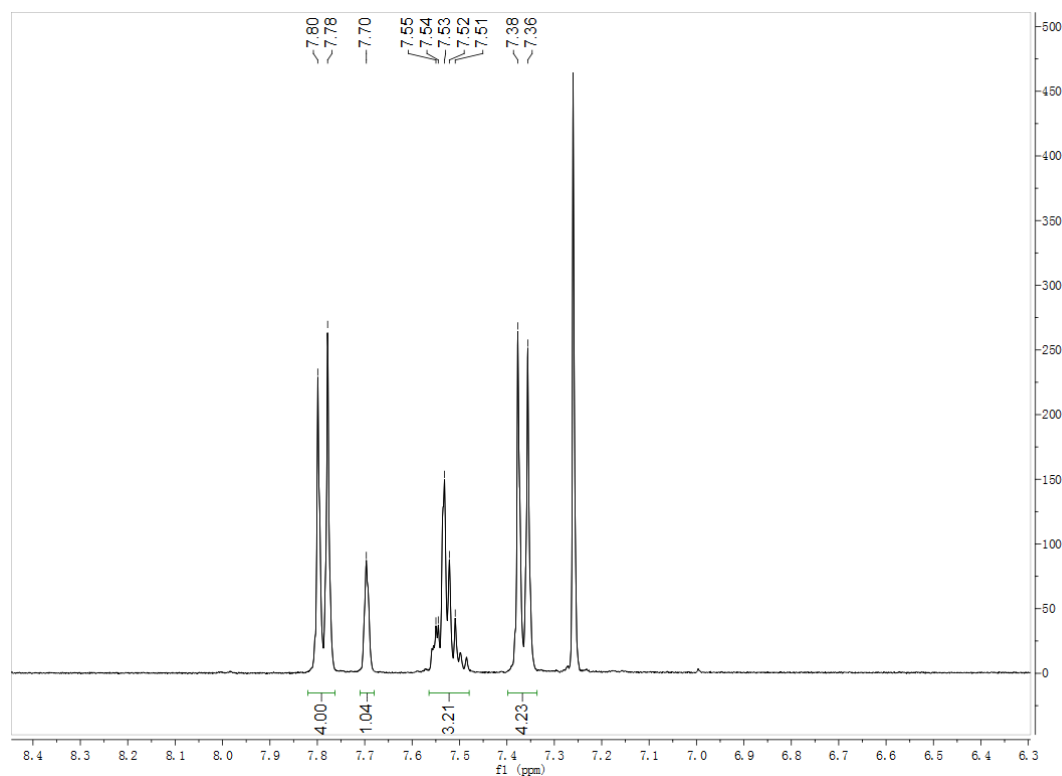
Supplementary Figure 7. 1H NMR spectrum of 4,4''-diiodo-1,1':3',1''-terphenyl in CDCl3.
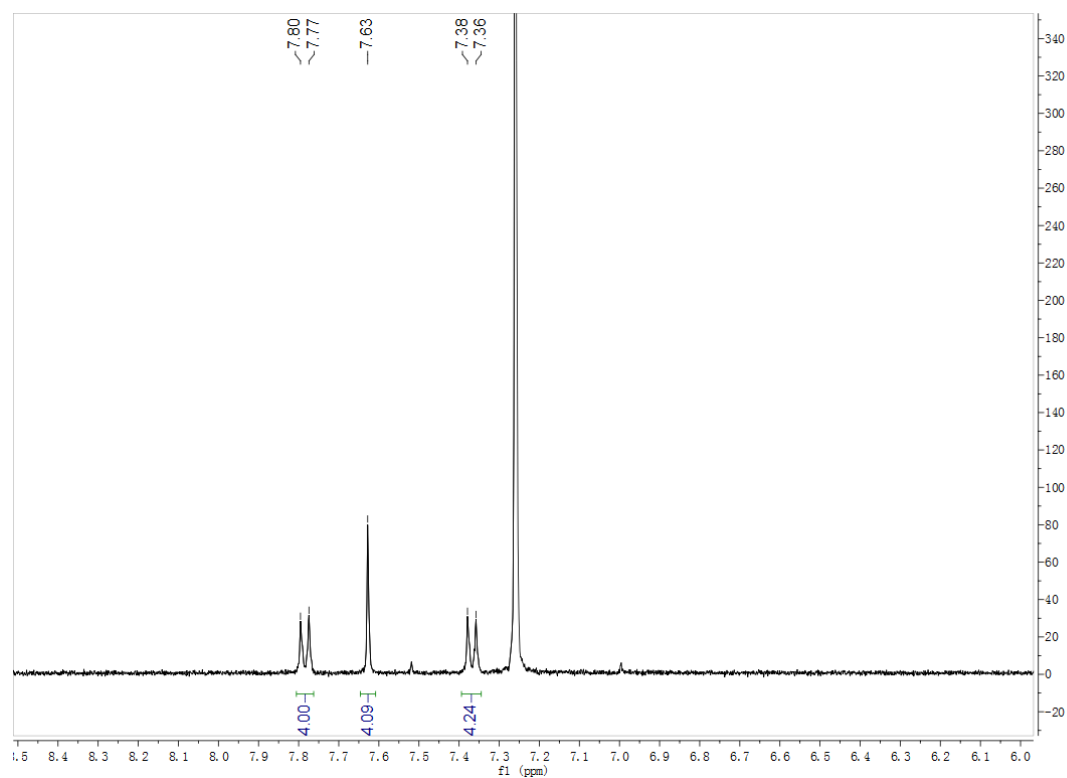
Supplementary Figure 8. 1H NMR spectrum of 4,4''-diiodo-1,1':4',1''-terphenyl in CDCl3.
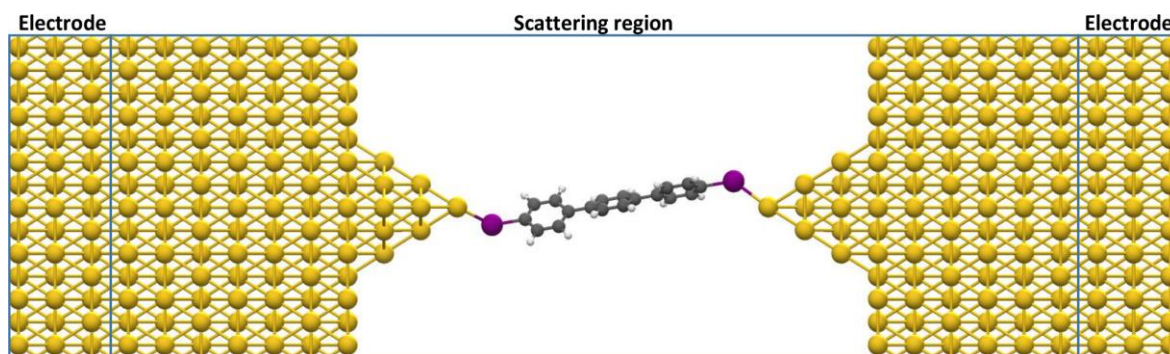
Supplementary Figure 9. Scattering region and electrode super cells.

First-principles transport calculations

Method

Electron transport properties of Para and Meta were calculated using a combination of

density functional theory (DFT) electronic structure calculations and non-equilibrium

Green's function techniques [5]. To obtain a self-consistent Kohn-Sham Hamiltonian under open boundary conditions we iterated the following procedure until self-consistency: (i) using the DFT Kohn-Sham Hamiltonian the corresponding density matrix is calculated within the Green's function formalism which accounts correctly for the open boundary conditions [5,6], (ii) from this density matrix in turn a new Kohn-Sham Hamiltonian is obtained using DFT. As this system is non-periodic in transport direction (parallel to the z-axis) we determined the self-consistent Hatree potential with the correct boundary conditions within the bulk electrodes (Fig. S9) using a multi-grid solver [7] with Dirichlet boundary conditions parallel and periodic boundary conditions perpendicular to the transport direction. This allowed us to ensure that the electrode Hartree potential matched correctly to the Hartree potential at the boundary of the scattering region, which included sufficiently large parts of the electrodes to ensure that the Hartree potential approaches bulk values.

From the self-consistent Kohn-Sham Hamiltonian the transport properties were obtained using the Landauer formalism [8,9]

$$I = \frac{2e}{h} \int \mathrm{d}E T(E,V)[f(E - \mu_L) - f(E - \mu_R)], \qquad \text{(S1)}$$

expressed in terms of Green's functions [10]

$$T(E,V) = \mathrm{Tr}[\boldsymbol{G}^r(E,V)\boldsymbol{\Gamma}_L^r(E,V)\boldsymbol{G}^a(E,V)\boldsymbol{\Gamma}_R^r(E,V)], \qquad \text{(S2)}$$

where e is the electron charge, h the Planck constant, $f(E - \mu_{L,R})$ the Fermi function of describing the electron distribution in the left (L) and right (R) electrode at the corresponding chemical potential $\mu_{L,R}$, and $T(E,V)$ the transmission function with $\boldsymbol{G}^r$ ($\boldsymbol{G}^a = (\boldsymbol{G}^r)'$) being the retarded (advanced) Green's function defined on the scattering region, and $\boldsymbol{\Gamma}_{L,R}^r(E,V)$ the spectral functions of the two electrodes. Under small bias

voltage conductance G is determined by the transmission at Fermi energy E_F and given by Eq. 1 in the main text.

DFT calculations

All DFT calculations were performed using the DFT code Conquest [11] at the PBE [12,13] level of theory using a SZP basis set derives from Hamann pseudo potentials [14,15]. A Monkhorst k-point grid of 5x5x1 was used for the calculation of the scattering region and 5x5x100 k-points for the electrodes, whereas the electrode super-cell consisted of 7x4x1 simple orthorhombic unit cells (a=5.45 a.u., b=9.44 a.u., and c=13.45 a.u.) of an Au fcc lattice in [111] direction (Supplementary Fig. 9). The energy grid cutoff was chosen to be 100 Har.

Contact geometries

The contact geometries were modeled as Au electrodes in [111] direction with atomic sharp tips connected to the molecule (Supplementary Fig. 9), where the molecule as well as the 6 innermost tip Au atoms were relaxed with a precision of 10^{-4} a.u.

References

1.   Hirayama, M.; Caseri, W. R.; Suter, U. W., Reaction of Long-Chain Iodoalkanes with Gold Surfaces. *Journal of Colloid and Interface Science* **1998,** *202* (1), 167-172.
2.   Yu, Y.; Dubey, M.; Bernasek, S. L.; Dismukes, G. C., Self-Assembled Monolayer of Organic Iodine on a Au Surface for Attachment of Redox-Active Metal Clusters. *Langmuir* **2007,** *23* (15), 8257-8263.
3.   Watts, J. F., High resolution XPS of organic polymers: The Scienta ESCA 300 database. G. Beamson and D. Briggs. 280pp., £65. John Wiley & Sons, Chichester, ISBN 0471 935921, (1992). *Surface and Interface Analysis* **1993,** *20* (3), 267-267.
4.   Some, S.; Sohn, J. S.; Kim, J.; Lee, S.-H.; Lee, S. C.; Lee, J.; Shackery, I.; Kim, S. K.; Kim, S. H.; Choi, N.; Cho, I.-J.; Jung, H.-I.; Kang, S.; Jun, S. C., Graphene-Iodine

Nanocomposites: Highly Potent Bacterial Inhibitors that are Bio-compatible with Human Cells. **2016,** *6*, 20015.

5.   Ke S.-H.; Baranger H.U.; Yang W.; Electron transport through molecules: Self-consistent and non-self-consistent approaches, *Phys. Rev. B* **2014**, 70, 085410

6.   Robert, v. L.; Gianluca, S. Nonequilibrium Many-Body Theory of Quantum Systems: A Modern Introduction; Cambridge University Press, 2013.

7.   Anton L.; Womack J.; Dziedzic J., DL-MG v 2.0.2 [Computer software]. Retrieved from https://ccpforge.cse.rl.ac.uk/gf/project/dl-mg/

8.   Landauer R., Spatial Variation of Currents and Fields Due to Localized Scatterers in Metallic Conduction*, IBM J. Res. Dev.* **1957**, 1, 233

9.   Büttiker M., Four-Terminal Phase-Coherent Conductance, *Phys. Rev. Lett.* **1989,** 57, 1761

10.   Yigal M.;. Wingreen N.S , Landauer formula for the current through an interacting electron region, *Phys. Rev. Lett. 1992, 68, 2512–2515*

11.   Bowler D. R.; Miyazaki T., Calculation for millions of atoms with density functional theory: linear scaling shows its potential, *J. Phys. Condens. Matter* **2010**, 22, 074207.

12.   Perdew, J. P.; Wang, Y., Accurate and simple analytic representation of the electron-gas correlation energy, *Phys. Rev. B* **1992**, 45, 13244–13249.

13.   Perdew, J. P.; Burke, K.; Ernzerhof, M., Generalized Gradient Approximation Made Simple, *Phys. Rev. Lett.* **1996**, 77, 3865–3868.

14.   Hamann, D. R. Optimized norm-conserving Vanderbilt pseudopotentials, *Phys. Rev. B* **2013**, 88, 085117

15.   van Setten, M. J.; Giantomassi, M.; Bousquet, E.; Verstraete, M. J.; Hamann, D. R.; Gonze, X.; G.-M., R. The PseudoDojo: Training and grading a 85 element optimized norm-conserving pseudopotential table, *arXiv:1710.10138* **2017**